

Shape memory-based gastric motility 3D mapping

Highlights

- A pressure sensor array is integrated with a coil-like Nitinol-supporting structure
- The probe is stretched and delivered via the esophagus into the stomach
- The body temperature drives the phase transition of the probe
- The probe conforms to the gastric cavity and delivers the sensors to the wall

Authors

Neil Zixun Jia, Qiyun Gao, Vítor Sencadas, ..., Ziliang Kang, Hen-Wei Huang, Giovanni Traverso

Correspondence

cgt20@mit.edu

In brief

A motility-mapping platform that maps 3D pressure distribution in the stomach is described.



Develop

Prototype with demonstrated applications in relevant environment



Jia et al., 2023, Device 1, 100010
July 21, 2023 © 2023 Elsevier Inc.
<https://doi.org/10.1016/j.device.2023.100010>

Article

Shape memory-based gastric motility 3D mapping

Neil Zixun Jia,^{1,10} Qiyun Gao,^{1,10} Vitor Sencadas,^{2,3} Michelle Zong,⁴ Jesse George-Akpenyi,¹ Sylvia E. Waft,¹ Johannes L.P. Kuosmanen,¹ Josh Jenkins,¹ Keiko Ishida,^{6,7} Alison M. Hayward,^{1,5,6,9} Wiam Abdalla Mohammed Madani,^{6,9} Niora Fabian,^{1,5,6} George Selsing,^{1,6,9} Stephanie Owyang,^{1,9} Khalil B. Ramadi,^{1,6,7,8,9} Ziliang Kang,^{1,9} Hen-Wei Huang,^{1,6,9} and Giovanni Traverso^{1,9,11,*}

¹Department of Mechanical Engineering, Massachusetts Institute of Technology, Cambridge, MA 02139, USA

²Department of Materials and Ceramic Engineering, CICECO–Aveiro Institute of Materials University of Aveiro, 3810-193 Aveiro, Portugal

³School of Mechanical, Materials, Mechatronic and Biomedical Engineering, University of Wollongong, Wollongong, NSW 2522, Australia

⁴Department of Material Science and Engineering, Massachusetts Institute of Technology, Cambridge, MA 02139, USA

⁵Division of Comparative Medicine, Massachusetts Institute of Technology, Cambridge, MA 02139, USA

⁶David H. Koch Institute for Integrative Cancer Research, Massachusetts Institute of Technology, Cambridge, MA 02139, USA

⁷Division of Engineering, New York University Abu Dhabi, Abu Dhabi, United Arab Emirates

⁸Tandon School of Engineering, New York University, New York, NY, USA

⁹Division of Gastroenterology, Brigham and Women's Hospital, Harvard Medical School, Boston, MA 02115, USA

¹⁰These authors contributed equally

¹¹Lead contact

*Correspondence: cgt20@mit.edu

<https://doi.org/10.1016/j.device.2023.100010>

THE BIGGER PICTURE Gastrointestinal (GI) motility processes and transports the food along the GI tract. Dysmotility, including gastroparesis and dyspepsia, affects 15%–20% of the general population. At present, clinical evaluation of gastric dysmotility is limited to radiographic methods that are able to provide information only on the rate of gastric emptying, but not pressure mapping within the stomach.

SUMMARY

Gastrointestinal (GI) dysmotility, caused by impaired muscular contractions in the GI tract, affects 15%–20% of the population. Current clinical evaluations are limited. Here we report a motility-mapping platform that maps three-dimensional (3D) pressure distribution in the stomach, addressing gaps in existing techniques, such as high-resolution manometry. We validated the platform's measurements against existing techniques in the esophagus and rectum. A sensor probe, designed to conform to specific anatomical environments, uses body-temperature-triggered shape memory alloy to adapt to the stomach. We tested the platform's motility mapping in swine stomachs, esophagi, and rectums, both *ex vivo* and *in vivo*. This 3D *in vivo* characterization could transform our understanding, diagnosis, and treatment of complex GI conditions, such as functional dyspepsia.

INTRODUCTION

Gastrointestinal (GI) motility, in which ingested material is mechanically transported through the GI tract, is essential to the digestion and processing of nutrients.^{1–3} There are two main types of motility reflexes: accommodation or distension,^{4,5} which refers to the GI tract's ability to expand or contract according to the volume of its contents; and peristalsis,^{6–8} which refers to the mechanical waves generated by the GI tract to propel and process food. The impairment of motility, also called dysmotility, is quite common, with a prevalence of 15%–20% among the general population.^{9,10} GI dysmotility underlies common disorders such as gastroesophageal reflux disease and chronic constipation. However, diagnostic methods remain limited, particularly for the study and evaluation of gastric motility.

Esophageal and anorectal motility are better understood than gastric motility, owing to the existence of high-resolution manometry (HRM) and impedance planimetry. In clinical practice, HRM is used in narrow, homogeneous, tubular organs¹¹ (e.g., the esophagus) in the evaluation for motility disorders. HRM involves a catheter with a densely packed pressure sensor array with a resolution of 1–2 cm and is capable of evaluating the spatial-temporal pressure distribution in a 2D format (pressure along a line). Information provided by HRM is critical for the diagnosis and management of esophageal dysmotility. For instance, the American Gastroenterological Association recommends HRM evaluation before antireflux surgery to rule out contraindications or esophageal motility disorders that cannot be treated with this type of surgery.¹¹ Similarly, anorectal manometry is commonly used in the evaluation of fecal incontinence or



constipation to guide further management, such as biofeedback therapy or surgical correction of disorders such as Hirschsprung's disease.^{12,13} Impedance planimetry¹⁴ is another technique used in the evaluation of esophageal motility, and it uses a plastic tube filled with saline and a catheter with an array of electrodes, with changes in tube diameter caused by contractions appearing as changes in electrical resistance between a pair of electrodes. However, these catheter-based techniques cannot be used in other parts of the GI tract that are not narrow and homogeneous, such as the stomach.

Evaluation of gastric motility in clinical practice is mainly limited to gastric emptying scintigraphy, which involves ingestion of a radiolabeled meal and measurement of the percentage of gastric retention at time points up to 4 h. This is useful for the diagnosis of gastroparesis, or delayed gastric emptying (defined as gastric retention >10% at 4 h).¹⁵ However, this method does not provide pressure mapping within the stomach. Wireless motility capsules¹⁶ can be used as an alternative to gastric scintigraphy, but they provide similar information on gastric emptying. These capsules are swallowed by patients and are capable of measuring pH, pressure, and temperature. Gastric emptying, small bowel transit time, and colonic transit time are estimated based on the pH profile (i.e., the rise in pH when moving from the stomach to the small intestine and a drop in pH when moving from the small intestine to the colon). Pressure readings are of limited clinical utility compared with manometry and are unable to detect a peristaltic pressure wave front.¹⁷ Importantly, patients with and without gastroparesis often experience functional dyspepsia, defined as ongoing symptoms (early satiety, postprandial fullness, bothersome epigastric discomfort) in the absence of structural etiologies such as peptic ulcer disease or acid reflux.¹⁸ Without a method to map spatial pressure distribution within the stomach, careful detailed evaluation of potential altered motility cannot be evaluated. Thus, the diagnosis of functional dyspepsia remains heavily symptom driven and not one that can be correlated with measurable biomarkers, such as changes in gastric motility or gastric contraction pressure.

A number of investigational motility-mapping systems have been developed in attempts to improve evaluation of motility throughout the GI tract. Electrode-recording systems are used to quantify the bioelectrical signals that correspond to motility. These systems have been used to directly measure the bioelectric slow waves in the GI tract in animal studies.^{19–23} However, these systems need to be surgically implanted, which limits their clinical application. There are efforts to record and analyze motility-related bioelectrical signals via noninvasive electrodes; however, the information acquired is limited to abstracted features of motility rather than global distributions.^{24,25} Another trend in motility-mapping systems is to replace solid-state pressure sensors with optical-fiber-based pressure sensors.^{26–28} Optical-fiber-based sensors enable sensing probes to be miniaturized. However, because sensors are still embedded into a catheter, like a traditional manometry probe, the data acquired from the two systems are effectively the same and limited to narrow tubular organs. Other sensing methods have also been used for motility mapping, including mutual inductance,²⁹ bioacoustics,³⁰ resistive sensing (e.g., thin-film strain gauges),³¹ magne-

toresistive sensing, and biosusceptometry.³² Previously, our group developed a flexible piezoelectric device that can conform to smaller segments of the stomach wall and monitor motility.³³ To the best of our knowledge, there is no system reported that is capable of achieving three-dimensional (3D) pressure mapping of the stomach.

A further complication in the challenge associated with developing a stomach motility probe lies in deploying sensors in the gastric environment with the constraint of passage through the narrower tubular esophagus, akin to the “ship in a bottle” challenge. A medical device must enter the esophagus with a diameter no larger than 2 cm but must expand in the gastric cavity to a maximum diameter of approximately 8 cm and deliver the sensor to the gastric wall. Existing stents are designed for tubular organs, such as arteries and the urinary tract, and have limited expanding capability. Gastric retentive devices have been designed but lack the ability to expand and deliver sensors to the gastric wall, including in our previous work.³⁴

To address these limitations in 3D mapping of gastric motility, we developed conformal pressure-sensing probes by carefully designing the shape, stiffness, and heat-transfer properties of the probe's supporting structure. The motility-sensing probes use nitinol, a shape memory alloy, for its conformal and adaptive supporting structure. Nitinol has been extensively applied in stent^{35–39} and gastric retentive devices,^{34,40} and it has been proven to be chemically safe and stable for *in vivo* applications. The design of the supporting structures is able to adapt to the anatomic and dimensional variation within stomachs across subjects. An array of pressure sensors is embedded into the probe, with a spatial resolution of 2 cm. The probes use flexible printed circuit (FPC) sensor belts, and an electronic interface is developed to read and process the data measured by all probes. Esophageal and rectal probes can be placed or removed via an endoscopic overtube or directly into the lumen. The stomach probe can be stretched into a long belt and delivered endoscopically. Once the probe is deployed, body temperature drives the phase transition of the nitinol-supporting structure from martensite to austenite state; it then transforms into its pre-programmed shape. Once the probe is placed into the subject, body temperature continuously heats the probe, and thus it is important to avoid phase transition from occurring before the probe is positioned. We found the deployment time of the stomach probe needs to be no more than about 4 min to avoid premature phase transition. Once the phase transition is complete, the pressure sensors are delivered to the wall of the GI tract. After testing is completed, the probes can be removed from the subject endoscopically without a surgical procedure. The platform was tested to measure changes in gastric pressure in swine. Because there is no clinically available system for mapping spatial-temporal pressure distribution within the stomach, this platform was also tested in the esophagus and rectum in swine and validated against a US Food and Drug Administration (FDA)-approved HRM¹¹ system, which is used clinically to obtain 2D intraluminal pressure data. The system not only integrates motility evaluation of three anatomic segments (esophagus, stomach, and rectum) of the GI tract into one platform

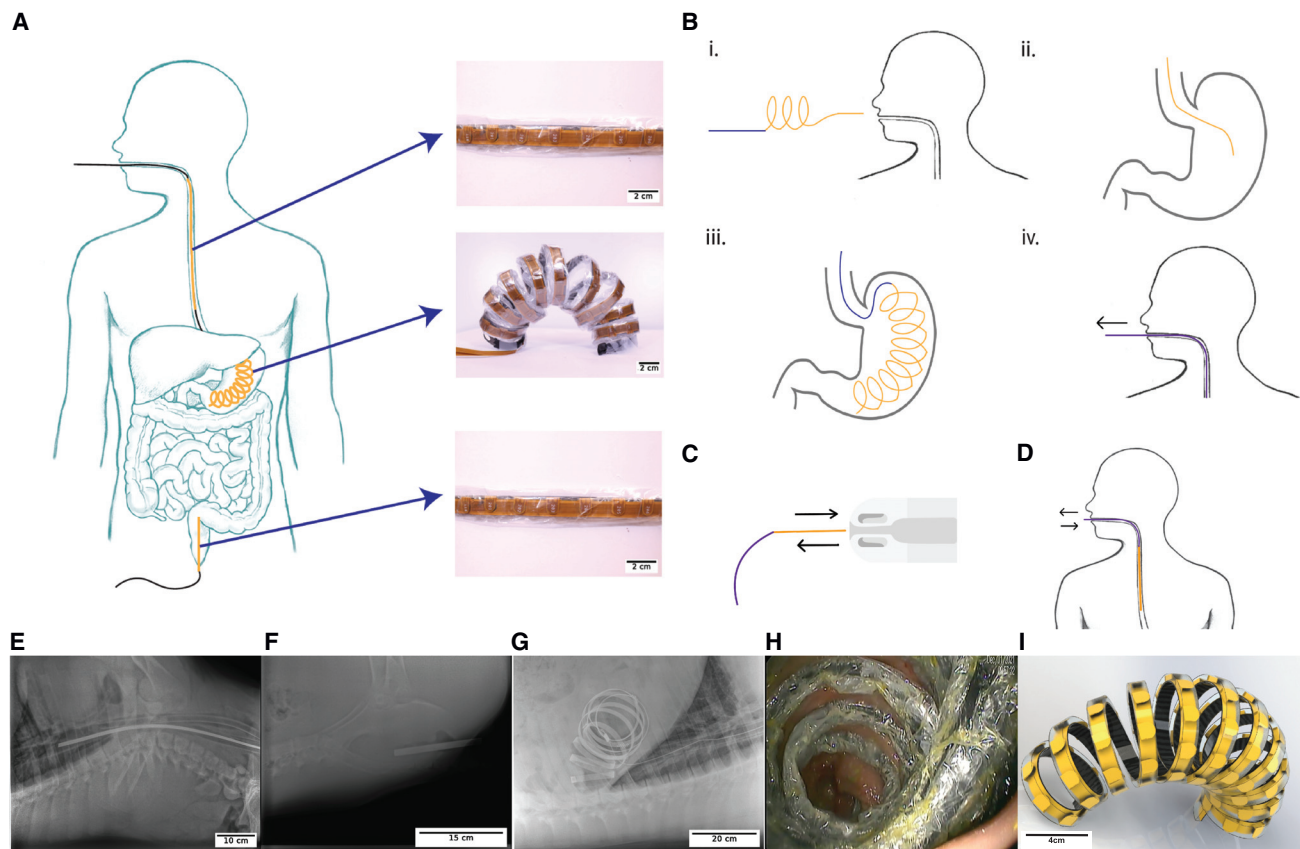


Figure 1. Adaptable motility probes

(A) Illustration of the universal motility-mapping system with tubular and bolus sensing probes.
 (B) Deployment and retrieval workflow of the stomach motility probe.
 (C and D) Deployment and retrieval illustrations of (C) rectum and (D) esophagus probe.
 (E and F) X-ray of tubular probe in (E) esophagus and (F) rectum.
 (G and H) X-ray (G) and endoscope image (H) of the bolus probe in the stomach.
 (I) Illustration of the bolus organ (stomach) motility probe.

but also achieves global motility mapping inside the stomach, which is not yet clinically available.

RESULTS

Adaptive motility-sensing probes

The platform developed in this work has three different probes that are designed to support mapping of the mechanical pressure in the stomach, esophagus, and rectum (Figure 1A). Linear sensor probes are used for the esophagus and rectum. To map the 3D distribution of mechanical pressure in the stomach, we envisaged and built a conformal globular supporting structure. To deploy the stomach probe, it is stretched into a linear belt and advanced through an endoscopic overtube placed inside the esophagus. Once the device is deployed inside the body, the body temperature from the subject triggers the nitinol phase transition (Figure 1B). The probe returns to the programmed shape and conforms to the stomach walls. To retrieve the device, a cable, which is attached to the probe, can be withdrawn; the device will then exit via the overtube in the esophagus (see

Figures 1C and 1D). The rectal and esophageal probes can be directly inserted into the rectum or via an overtube into the esophagus, respectively. Cables attached to either rectal or esophageal probe can be withdrawn; the probes then exit the subject. Figures 1E–1G show X-ray images of the probes in the esophagus, rectum, and stomach of a swine, respectively. An endoscopic image of the probe deployed in the stomach of the swine is shown in Figure 1H demonstrating the coil-like structure (Figure 1I) and juxtaposition with the gastric mucosa. The sensing units are delivered to the stomach wall and pushed against by the supporting structure (Figure 1H). Endoscopic and radiographic evaluation did not reveal mucosal injury as supported by the lack of abrasions, as well as free air in the abdomen (Figures 1E–1H).

Self-aligned supporting structure for motility probes

The probes use the shape memory alloy nitinol as the supporting structure material. The nitinol strips used for the esophagus and rectum probes are 1 mm thick, 12 cm (rectum probe) or 54 cm (esophagus probe) long. Using the dimensions measured from

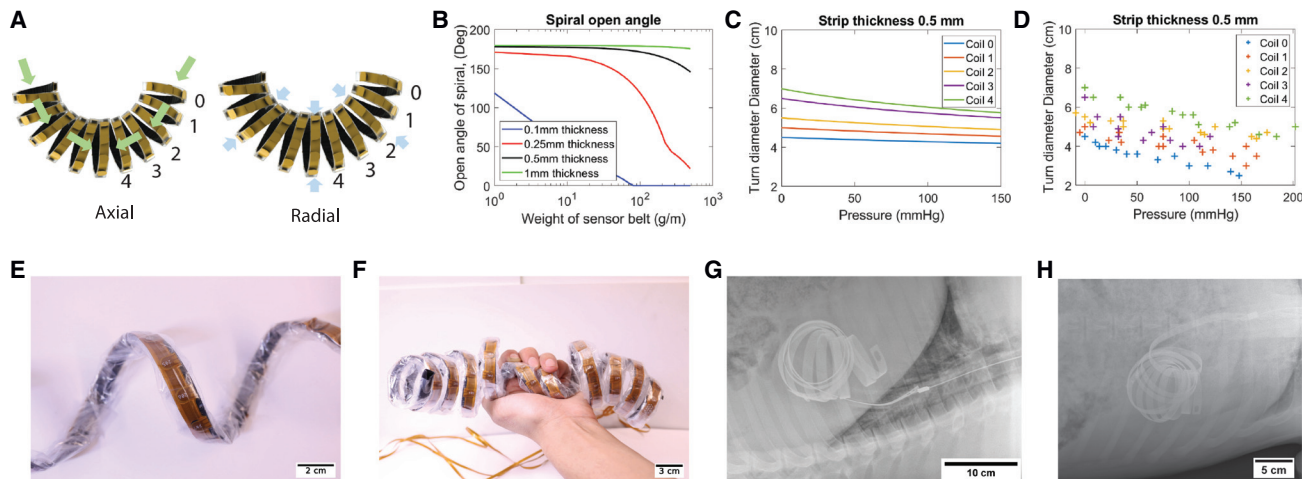


Figure 2. Mechanical design of the supporting structure

(A) The illustration of axial and radial forces bolus probe experienced inside the stomach.

(B and C) Models for bolus organ-supporting structure: (B) axial stiffness model result and (C) radial stiffness model result.

(D) Change of diameter of each turn when a uniform load is applied to the supporting structure. Each cross (+) refers to a data point obtained from the radial stiffness testing experiment.

(E) Stomach probe being extended.

(F) Stomach probe being crushed by hand.

(G and H) X-ray of supporting structure inside the stomach of (G) 89-kg and (H) 90-kg pigs.

a swine stomach (Figure S1A), we found that to have a 2-cm resolution of pressure mapping in the stomach, similar to the FDA-approved manometry's resolution (22), there should be ~ 90 sensing units. Thus, we designed a coil-like structure 180 cm long (Figure 1I). The challenge in building a conformal supporting structure is achieving an appropriate axial stiffness while minimizing radial stiffness. Axial stiffness is the structure's ability to expand inside stomach against its weight (Figure 2A). The probe needs to be stiff enough axially to expand across the stomach. Radial stiffness is the structure's ability to push against the surrounding stomach tissue (Figure 2A). The probe's radial stiffness needs to be minimized so the probe can adapt to subjects with different stomach shapes/sizes.

A model was built to study the influence of the thickness of the nitinol on axial stiffness. Nitinol sheets with a transition temperature of 35°C and thicknesses of 0.1, 0.25, 0.5, and 1 mm were selected. The width of the strip was set at 1 cm in order to fit inside an overtube with a diameter of 1.5 cm. As shown in Figure 2B, with a sensor belt that weighs 100 g/m, a 0.1-mm-thick device fully collapses. Devices with thicknesses of 0.25, 0.5, and 1 mm have open angles of, respectively, 100°, 175°, and 179°, as illustrated in Figure S1B. We found the optimal thickness to be 0.5 mm, because it allows a large open angle (expansion across the stomach) with the smallest thickness. In our coil spring model of radial stiffness, the diameter of each turn is a function of the pressure uniformly applied to the coil, which comes from the gastric wall, and the result is shown in Figure 2C. In the experimental data, as shown in Figure 2D, one can see from 0 to 150 mm Hg, and the diameter of each turn is reduced by ~ 2 cm. See [experimental procedures](#) in the SI for more information of axial and radial stiffness models and of stiffness testing. Considering the diameter of a 75- to 100-kg swine's stomach is 4–7 cm, the supporting struc-

ture is able to reduce total diameter by 30% to 50% when the maximum possible pressure is applied. This indicates that the radial stiffness of the supporting structure is sufficiently small.

The supporting structure with 0.5 mm thickness is then fabricated and integrated with the sensor belt. The probe is stiff but flexible, which allows it to be stretched or compressed for adaptation purposes (Figures 2E and 2F). We then deployed the same supporting structure into animals with different body weights. Figures 1G, 2G, and 2H are X-ray images of the supporting structure in swine of body weight 103, 89, and 90 kg, respectively. One can see the supporting structure has aligned by itself and adapted to stomachs of different subjects.

To ensure the safety of the intervention, we needed to understand the frictional forces during the deployment and retrieval processes (details provided in the [experimental procedures](#) section in the SI). Figures S1C and S1D show the frictional force on the supporting structure in the overtube as a function of how far it has been pushed/pulled into/out of the overtube. Figure S1C shows the friction when the structure is in the martensite phase (below the phase transition temperature) and pushed into the overtube. The frictional force reaches a maximum value of 27 N with a coefficient of friction of 0.2. Figure S1D shows the frictional force when the supporting structure is in the austenite phase (above the phase transition temperature) and removed through the overtube. In the austenite phase, the maximum friction force reaches 70 N with a coefficient of friction of 0.2. In both cases, the maximum frictional force is proportional to the coefficient of friction. Our findings have two implications. First, the device must be well lubricated in both the deploying and retrieval processes. In the *in vivo* experiment, we used an edible oil spray (PAM Cooking Spray) to create an oil-rich environment in the overtube. Second, in the deploying process, we needed to

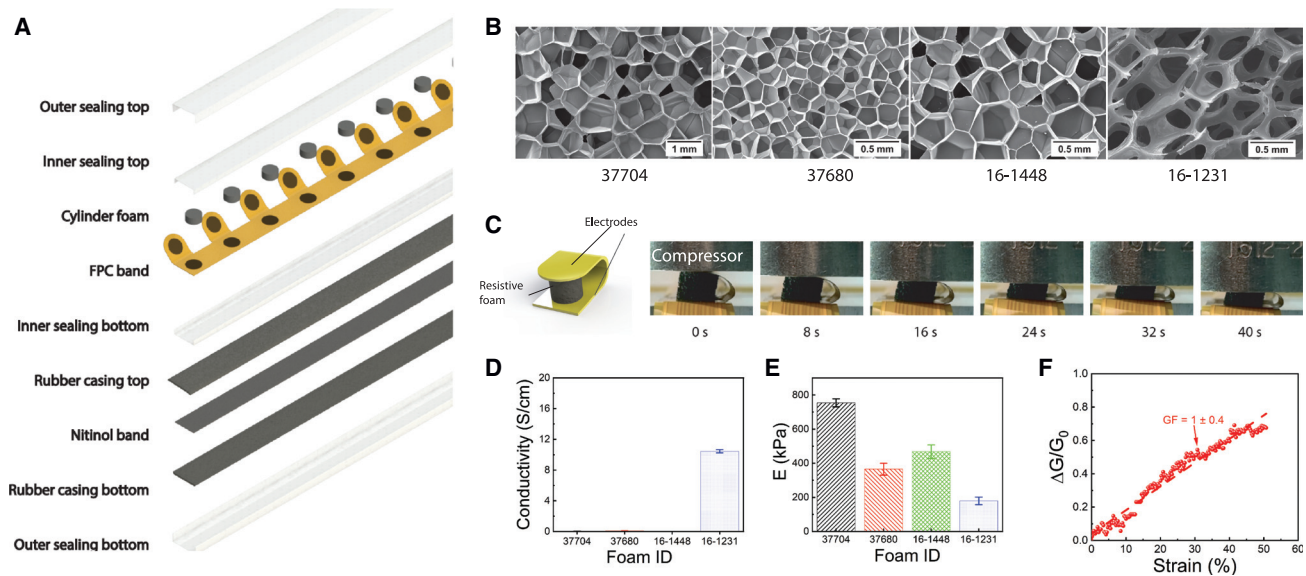


Figure 3. Pressure-sensing units design and system integration

- (A) Exploded view drawing of motility probe.
 (B) SEM images of the foams (37704-ND, 37680-ND, 16-1448-ND, and 16-1231-ND).
 (C) Single cell under compression test on the Instron platform.
 (D and E) Properties of four off-the-shelf anti-static packaging foams: (D) conductivity and (E) Young's modulus.
 (F) Gauge factor of foam 16-1231.

ensure the transition from the martensite to austenite phase would not occur before reaching the stomach. A heat transfer model was developed to study the temperature of the device as a function of the time in the body of the swine (Figure S1E) (heat-transfer mathematical model is described in the [experimental procedures](#) in the SI). The body temperature of the swine is 38.6°C–39.2°C.⁴¹ The plateau in the graph is the time period when the device reaches the transition temperature. The heat is absorbed into the material as latent heat to drive the phase transition. Before the plateau, the device's temperature rises from the initial room temperatures, set at 15°C, 20°C, 25°C, and 30°C. To minimize friction and prevent the probe from undergoing phase transition in the overtube, the probe needs to reach the stomach before t_p , which is when the phase transition starts. With an overtube length of 0.5 m, the total allowable delivery times with different initial room temperatures are shown in Table S1.

Sensor probe prototyping and integration with supporting structure

Each of the probes has a linear pressure sensor system composed of a FPC, a nitinol strip as the supporting structure, and two layers of sealing for impermeability (Figure 3A). The probes require no microfabrication or clean room process. The probes are fabricated entirely using off-the-shelf materials and thus can be easily scaled up in production. To design the conformal GI tract motility-mapping probes with piezoresistive sensors, we needed materials with low elastic modulus and high electrical conductivity. To build a sensing unit, we evaluated commercially available anti-static foams and fabricated multi-

walled carbon nanotube (MWCNT)-doped polymers (see Figures 3B and S2). An off-the-shelf anti-static foam was used as the sensing material because of its high electromechanical performance and strong adhesion to the FPC board. MWCNT-doped foam's electromechanical performance could be tuned to the desired values for motility-mapping application. However, its poor adhesion with the Cu electrodes on the FPC prevent the MWCNT-doped foam from being implemented in the sensing probe.

The piezoresistive foam's electrical resistance decreases when the pressure is applied uniaxially onto it. To understand the mechanism of this phenomenon, we first studied the microstructure of the piezoresistive foams and then characterized the electromechanical characteristics of the foams. As can be seen from the scanning electron microscopy (SEM) images in Figure 3B, all four foams exhibit a porous structure, with the pore diameter of 0.5–1 mm. The 3D morphology was evaluated using a 3D model from CT scan imaging data with 3- μ m resolution (Figure S3A). All piezoresistive foams had a porosity of over 90% (Figure S3B). The morphology and the porosity data helped us to build a hypothesis of anti-static foams' mechanism of detecting mechanical pressure. In the neutral state, where there is no pressure applied on the foam, the electrons flow through the skeleton of the foam. Once the foam experiences stress, the porous structure collapses and contacting points are created inside the foam. With a larger stress, more contacting points are created; thus, the electrical resistance of the foam decreases. In order to measure the electrical conductivity of the foams, a pair of flexible electrodes are attached to either side of the piezoresistive foam cylinder, as shown in the illustration of

Figure 3C. These electrodes enable the measurement of foams' I–V curves and electrical conductivity. For the measurement of mechano-electrical response and gauge factor (GF), the piezoresistive foams with flexible electrodes are placed under the compressor of the Instron, which applies forces at programmed speed and value. It is worth noting that in the measurement of stress-strain curves of the foams and Young's modulus, the foams are placed directly under the compressor without flexible electrodes. Additional details about the foam characterization can be found in the [experimental procedures](#) section in the SI.

The conductivity of the sample 16–1231 was superior to the other foams ([Figure 3D](#)). Sample 16–1231 had a conductivity of 10 S/cm, whereas other foams have significantly smaller conductivity. The foam 37704-ND had the highest Young's modulus value ($E = 754 \pm 24$ kPa), whereas the softer foam (16-1231-ND) had a value of $E = 180 \pm 22$ kPa ([Figure 3E](#)). In our application, the desired value for E is ~ 100 kPa because with a motility compression pressure of ~ 40 kPa, the material will have a significant deformation and thus a change of electrical resistance. The desired conductivity of the material is ~ 10 S/m. With this conductivity, the measured current would be ~ 1 mA when ~ 10 V of bias voltage is applied onto the sensing material. This amount of current is large enough for an accurate electrical resistance scanning (the resolution of current measurement is ~ 1 μ A in our system) while maintaining the voltage below the dangerous threshold of 30V.⁴² Based on our results, we concluded that the best candidate was the sample 16-1231-ND, with its low Young's modulus E ([Figure 3E](#)) and high electrical conductivity ([Figure 3D](#)). The piezoresistive behavior of the foam 16-1231-ND exhibited good linearity up to 50% deformation, with a GF value of 1.0 ± 0.4 ([Figure 3F](#)). A twin-spring model is developed to optimize the geometric parameters of the sensor cell, where the foam is modeled as a linear spring connected in parallel with the FPC modeled as a U-turn spring. The model is verified by observing the mechanical behavior of the sensor cell ([Figure 3C](#)). When the sample is compressed, the foam cell shrinks in height and behaves like a linear spring, and the diameter of the U turn gets smaller. The sensor is applied to 18 cycles of compression to verify its response linearity and a further 1,000 cycles to confirm its durability (see [Figures S3D](#) and [S3E](#)). The experimental data are in accordance with the twin-spring model prediction (FPC U-turn and the foam are modeled as two springs connected in parallel, see [supplemental information](#) for more information). Furthermore, foam 16–1231, which is used in this work for *in vivo* applications, is cross-linked polyurethane, carbon black, and acrylic-impregnated materials. All three compounds are found to be safe and non-cytotoxic.^{43–45}

In vivo evaluation of the motility-mapping probes

The probes were evaluated in the esophagus, rectum, and stomach in a swine model. Through endoluminal stimulation from either a balloon or dilation catheter, we observed the patterns of a single strong contraction followed by series of weaker contractions in the esophagus. To evaluate the performance of the esophageal probe, we applied a model food bolus (endoscopic placement of a balloon) and quantitatively compared the pressure readings ([Figure S4A](#)). In this study,

we utilized a 0–1 correlation factor to quantify signal similarity, where a correlation coefficient of 0 indicates no correlation and a coefficient of 1 indicates complete similarity between signals. The peristalsis peaks were captured by both the esophagus-sensing probe and a commercial HRM, which served as a comparator, with correlation factors of 0.581, 0.486, and 0.487 at 18, 20, and 22 cm from the incisors, and p values of the Wilcoxon rank-sum test of 4×10^{-17} , 5×10^{-8} , and 2×10^{-8} , respectively. The spectral intensity graph of the two sensing readings is shown in [Figure S4B](#). The correlation between the two spectra is 0.6645. The pressure-time-location graphs from 10 to 36 cm are shown in [Figures S4C](#) and [S4D](#). A clear similarity can be seen in the two graphs, in which three strong pulses are observed at $t = 0, 35,$ and 90 s with subsequent periodic contractions. We then used a dilation catheter to stimulate a single pulse of contraction in the esophagus. [Figure S4E](#) shows the strong single pulse captured by both devices, with correlation factors of 0.5578, 0.5597, and 0.6120 at 18, 20, and 22 cm from the incisors, respectively, and p values of the Wilcoxon rank-sum test of 5×10^{-6} , 1×10^{-5} , and 2×10^{-6} , respectively. The spectral intensity graph of the two devices is shown as [Figure S4F](#), with a correlation factor of 0.6202 for the two signals. The pressure-time-location graphs of the dilation catheter case are shown in [Figures S4G](#) and [S4H](#). A single strong pulse was recorded in both devices, followed by the subsequent smaller pulses.

In addition, we evaluated an endogenous reflex in the rectum called the rectoanal inhibitory reflex, which involves relaxation of the internal anal sphincter in response to rectal distention to facilitate the passage of stool.⁴⁶ We placed a balloon into the rectum of the swine along with the sensing probe and the HRM catheter. We inserted the balloon at 80 s (see [Figure S4I](#), annus panel), and thus at the anus there was a significant increase of pressure at around that time. This insertion was also captured by the sensing probe at location = 4 cm shown in the blue line. At 140 s, we inflated the balloon to simulate rectal stool filling. The filling was accompanied with a decrease in pressure at the level of the anal canal (see [Figure S4I](#), annus panel 140 s). The data from the rectum pressure mapping are presented in pressure-time-location graphs in [Figures S4J](#) and [S4K](#). The inflation event, which corresponds with an increase of pressure, occurs at 140 s at 4 and 6 cm; the relaxation event in the anus at 0 cm occurs around the same time point. More information regarding the experimental protocols can be found in the [experimental procedures](#).

The coil conformal arrangement was evaluated *in vivo* in the stomach of swine. Testing was performed through external abdominal palpation. A force sensor was placed under the hand to record the pressure applied by the hand. Sensing unit 24 on the probe was selected for comparison with the external pressure, and concordant pressure changes were observed. The pressure distribution of the device as a function of time is shown as well. As can be seen, external compression causes a pressure increase in two areas: on the distal lesser curvature and on the proximal greater curvature ([Figure 4A](#); [Video S1](#)). We also evaluated the effect of repeated gastric insufflation with a period of around 30 s ([Figure 4B](#)): each peak in the graph relates to a deflation event. During the deflation events, we had

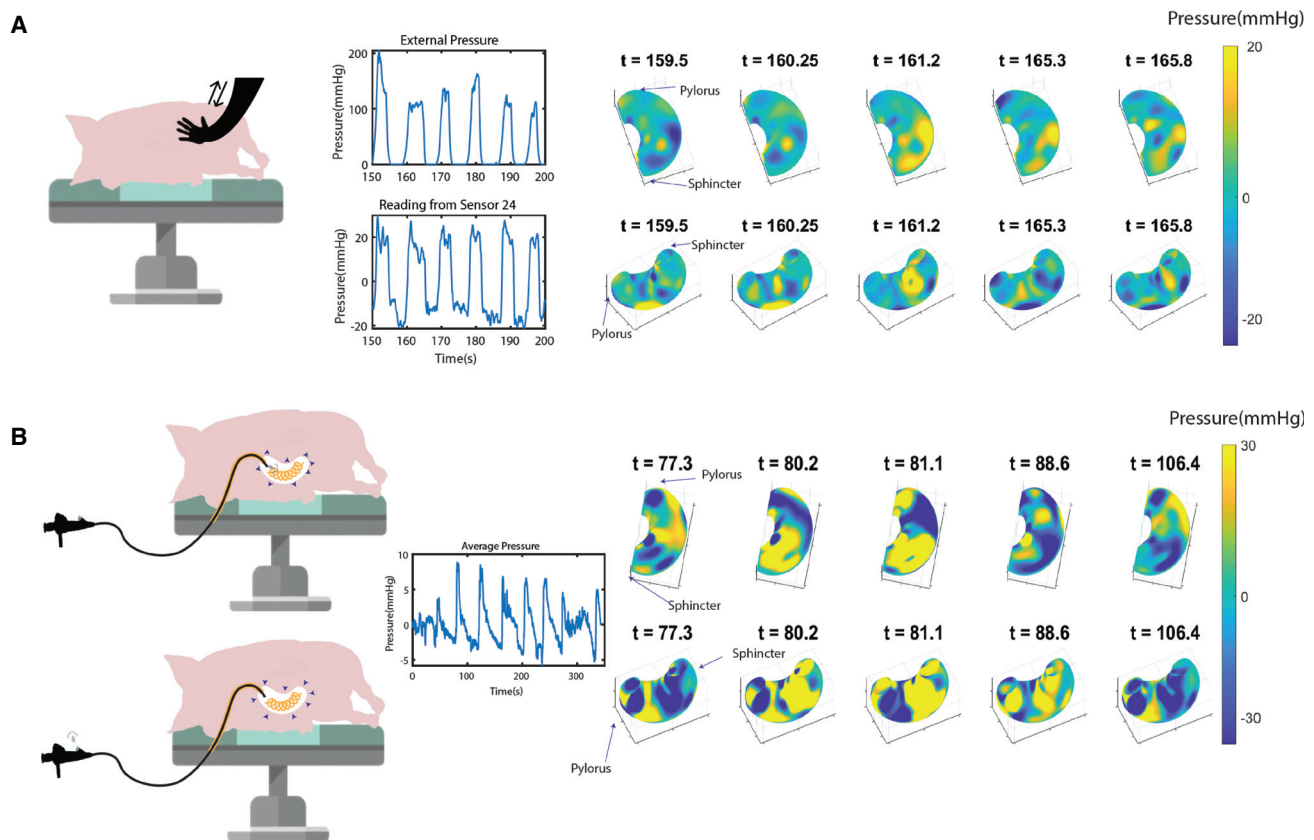


Figure 4. In vivo validation of stomach motility probe

(A) Application of external force on the abdomen of the swine via palpation. External pressure and reading from sensor 24 are plotted into two separated line plots. The mapping results at different time points are shown by contour graphs on the right.

(B) Applications of internal force by inflating and deflating the stomach with an endoscope. The average pressure from all sensors is plotted into a line graph. The mapping results at different time points are shown by contour graphs on the right.

the capacity to observe discrete changes throughout the gastric walls (see [Video S2](#)). We also studied the influence of azithromycin on gastric motility pattern (see [experimental procedures](#) section and [Figure S5](#)).

DISCUSSION

Here we report the development of a conformal motility-mapping platform that can measure 3D global pressure distribution in the GI tract. This platform is able conform to anatomic and dimensional variation across subjects, and it demonstrates the ability to evaluate changes in pressure within the stomach, esophagus, and anorectal canal. To achieve measurements of pressure in these distinct areas, we employed a shape memory metal (nitinol) support coupled to sensing arrays. The sensing probes use thin nitinol strips, designed according to the anatomic shape/dimension of the GI tract, as supporting structures and can be linearized to support endoluminal deployment. Linear nitinol strips are used as supports in esophagus and rectum probes. The supporting nitinol of the stomach probe is pre-programmed into a coil-like structure. Once the probe is inside the body, the thermal energy from the subject triggers the phase

transition in the nitinol, and the probe then conforms to the shape of the stomach. The probes deliver pressure-sensing units to the luminal wall and map the motor patterns. Upon completion, all three probes can be retrieved by withdrawing a cable connected to the probe. Through *in vivo* swine studies, we benchmarked the performance of the system to an FDA-approved HRM catheter through pressure mapping in the esophagus and rectum. The accuracy of the stomach-sensing probe was confirmed by applying known external and internal forces to the animal and measuring the resulting pressure distribution.

In our benchtop prototype, the maximum width of the sensing probe is 1 cm. Based on the *in vivo* study in the swine model, this probe is small enough to support deployment and retrieval. Given that the maximum diameter of an FDA-approved HRM probe is 4 mm, future work will be focused on further miniaturization of the system.

Commercial HRM has shown a lower noise compared with our probes. The sensor probes used in our work are benchtop prototypes assembled by academic researchers. Such “hand-made” fabrication lacks the manufacturing consistency that large corporations excel in. Also, we built our probes using widely available components such as low-cost op-amps,

resistors, and multiplexers, resulting in a low electronics cost. Future study and optimization will need to address the fabrication consistency and electrical noise observed with these early proof-of-concept prototypes.

The dimensions of the stomach sensing probe are highly dependent on the size of the stomach, and the nitinol support has the capacity for future personalization depending on body habitus of the subject. In this work, we designed the supporting structure based on the dimensions of the stomach in a 75- to 100-kg female swine model. In the current prototype the sensors were directly attached to the supporting nitinol band. In the future, further personalized measurements could decouple these elements.

Evaluation of gastric motility in clinical practice is limited to evaluation of gastric emptying only. However, patients without delayed gastric emptying or any structural abnormalities commonly experience a constellation of symptoms described as “functional dyspepsia,” which is poorly understood. This is due to the uncertain correlation between perception of discomfort and changes in gastric motility/pressure, for which evaluation is limited because there is no existing method to map spatial pressure distribution within the stomach. We have developed a device capable of mapping gastric pressure in a minimally invasive manner, which may be applied to human investigations in the future. This may enable correlation of symptoms with changes in gastric motility patterns, which has the potential to transform our understanding, diagnosis, and treatment for patients with yet-to-be defined gastric motility disorders.

The introduction of a motility probe may create a false sense of fullness, which can affect the device’s ability to measure natural motility patterns accurately. However, generating natural motility patterns has proven to be challenging in our study, which is limited to three sedated swine. Sedation is known to dampen GI motility,⁴⁷ reducing GI motility in sedated large mammals. Even with the infusion of azithromycin, a recognized prokinetic, a natural contraction pattern was not observed in our experiments. Most motility tests in clinical settings are conducted while patients are awake, which may lead to a more accurate representation of natural motility patterns. Current *in vitro* and *ex vivo* models apply mechanical modes of contraction/compression of tissue as models. We recognize the importance of evaluation in awake pre-clinical and clinical models. Toward optimal translation, future development may include percutaneous gastric access via a gastrostomy port, as well as early clinical trials in awake subjects.

Although endoscopic and radiographic evaluations have not revealed any mucosal injuries caused by the device, the degree of discomfort or gastric outlet obstruction that it may cause to patients remains unknown. Therefore, further studies are required to subjectively evaluate and minimize any discomfort or evidence of functional obstructions transiently associated with the device.

Future successful translation of these technologies will require further evaluation across a range of disease states, as well as further development on fabrication techniques and exploration of the potential for personalized probes that maximize data collection across a range of subject body habitus.

EXPERIMENTAL PROCEDURES

Resource availability

Lead contact

Further information and requests for resources and reagents should be directed to and will be fulfilled by the lead contact, Giovanni Traverso (cgt20@mit.edu).

Materials availability

This study did not generate new unique reagents.

Data and code availability

All data needed to evaluate the conclusions in the paper are present in the paper and/or the [supplemental information](#). Additional data related to this paper may be requested from the authors. This paper does not report any original code or algorithms. Any additional information required to reanalyze the data reported in this work is available from the lead contact upon request.

Materials involved

3D models of the platform were designed in Solidworks (Dassault Systemes, Velizy-Villacoublay, France). The manufacturing G-code was generated from Fusion 360 (Autodesk, San Rafael, CA, USA). The Tormach 440 PCNC (Tormach, Waunakee, WI, USA) was used to mill a plastic fixture. The raw material of the fixture was purchased from McMaster-Carr (McMaster-Carr, Elmhurst, IL, USA). The circuits were designed on Eagle PCB (Autodesk) and manufactured by Bittele Electronics (Markham, Ontario, Canada). Other relevant electronic components were purchased from Digi-Key Electronics (Thief River Falls, MN, USA). LDPE tubings were purchased from Uline (Pleasant Prairie, WI, USA). Eco-flex silicone was purchased from Smooth-On (Macungie, PA, USA). Tetrahydrofuran was purchased from Sigma-Aldrich (St. Louis, MO, USA). Styrene-ethylene-butylene-styrene polymer was supplied by Kraton (Houston, TX, USA). Multiwall carbon nanotubes were purchased from US Research Nanomaterials (Houston, TX, USA). The nitinol alloy was purchased from Kellogg’s Research Labs (Salem, MA, USA), and water jetting was done on an OMAX water jetting machine (Kent, WA, USA). Yorkshire swine used for *in vivo* studies were acquired from Cummings School of Veterinary Medicine at Tufts University (Grafton, MA, USA). The data visualization and processing were performed on MATLAB (MATLAB, Natick, MA, USA). The Universal Testing Machines was purchased from Instron (Norwood, MA, USA).

The *in vivo* swine experiments were pre-approved by the Massachusetts Institute of Technology (MIT) Committee on Animal Care, in accordance with all local, state, and federal regulations. All experiments were conducted according to the approved protocols.

Deploy/retrieval protocol of the stomach probe

The bolus probe was deployed and retrieved through via upper endoscopy. During deployment (see [Figure 1Bi](#)), we placed a lubricated overtube via the esophagus into the stomach. We unwound the probe (shown in orange) and began to push it through the overtube. Note that there’s a wire attached to the coil at the end (shown in blue). We continued pushing the coil through the esophagus (see [Figure 1Bii](#)) until the coil was fully in the stomach. We confirmed it with videos from the endoscope. Once the nitinol was in the stomach, it coiled back into its programmed shape because of the temperature in the body (see [Figure 1Biii](#)). When the coil was ready to be removed, we pulled the string attached to it until all the equipment was fully out (see [Figure 1Biv](#)).

IN VIVO EVALUATION PROTOCOLS ON A SWINE MODEL

To validate the proposed concept, we used three Yorkshire swine, each weighing 75–100 kg, to test the platform. During the experiments, all three probes were deployed into the swine, and an electronic connection cable transmitted signals from the individual sensor units to the scanning interface. Data were then streamed to a PC as shown in [Figure S13](#). An electronic interface is developed to record the data streamed from *in vivo* probes.

A clinical HRM was used as the tool of calibration and comparison. The swine were anesthetized before the experiment, and

several stimulation methods were used to generate motility/reflex. The *in vivo* data collected in this study is processed in MATLAB using moving average filter to remove the noise came from heart beating in the animals. To conduct *in vivo* experiments, we first deployed the sensing probes and HRM probes into the animals. The sensing and HRM probes were positioned next to each other, as illustrated by the blue curve in Figures S4A, S4E, and S4I. The sensing units on our probes are spaced 2 cm apart, while those on the HRM probe are spaced 1.5 cm apart. Both probes provide line mapping of contraction in the esophagus and rectum. To compare the data obtained from these probes, we highlighted data from three points in Figures S4A, S4E, and S4I. By doing so, we can determine the correlation between the measurements obtained from our sensing probes and those obtained from the HRM probe. We turned on the devices and observed the live-streamed baseline readings of HRM and sensing probes for 1–2 min. After confirming there were no motility/peristalsis/reflex patterns observed on both devices, we then subsequently started applying stimulations to the animals.

Animal sedation

Pigs were sedated with intramuscular injection of midazolam 0.25 mg/kg with dexmedetomidine 0.03 mg/kg and after intubation, anesthesia was maintained with isoflurane (1%–3% in oxygen).

Recovery

Pigs are returned to their pen and sedation reversed intramuscularly with the reversal agent atipamezole. If intubated, the pig is closely monitored until extubation and then is followed by monitoring of the recovery process until the pig is standing and considered bright, alert, and responsive (BAR).

Monitoring/Vitals throughout the study

After the pig is sedated and weighted, it is placed on a heated operating table with the additional thermal support of a heated blanket. Ophthalmic ointment is applied to both eyes. Once the pig is placed on isoflurane (1%–2%) and oxygen (1%–3%) either via a face mask or an endotracheal (ET) tube, it is then connected to an anesthesia monitoring machine in order to monitor vital signs every 15 min until returned to the pen.

Endoscopic delivery

Device delivered to stomach via colonoscope placed in orogastric tube/overtube. PENTAX EC-3870TLK (160 cm) for delivering drugs/devices to the stomach of larger pigs (>50 kg) and for retro flexing to visualize the entirety of the stomach.

Overtube specifications

The overtube specifications were as follows: material, urethane polyvinyl chloride (PVC); inner diameter, 5/8 inch; outer diameter, 3/4 inch; and wall thickness, 1/16 inch.

Stomach

Once the nitinol coil was in the stomach, we conducted three tests: internal force, external force, and azithromycin (USP) infusion. For internal force, we secured a hose clamp on the end of the overtube so that the stomach was a closed system.

Using the endoscope, we then inflated the stomach for 30 s and then deflated the stomach for 30 s. External force was applied by applying palpation on the abdomen. On the abdomen was a pressure sensor, whose calibration is depicted in Figure S5A. We obtained this calibration graph with an Instron measuring force and multimeter measuring resistance simultaneously. Tests for external force were conducted for 10 min in cycles, where each cycle consisted of 5 s of application and 10 s of rest.

While the sensing probe was in the animal's stomach, we infused 500 mg of azithromycin intravenously over 30 min using a syringe pump. The average pressure reading from the stomach sensing probe is shown in Figure S5B. We observed an increase in pressure during the first 20 min of infusion followed by a period of relaxation. Measurements from all 90 sensors are shown in Figure S5C, as raw data, and Figure S5D, after applying a moving average filter. In Figure S5C, we observed a very distinct respiration pattern. In Figures S5E and S5F, the height plot of the data from Figure S5D and the 3D interface of the pressure distribution show a migration pattern. However, when comparing the peristalsis patterns in Figure S5E and S5F, we did not find any significant differences between the beginning of the infusion versus 25 min afterward. The pressure distribution inside stomach is shown in Figure S5G. Therefore, it does not appear the migration pattern is caused by azithromycin.

Esophagus

To verify the accuracy of our device, we conducted comparison studies in the esophagus. First, we tested the effect of a bolus balloon on esophageal peristalsis, which simulates food bolus. We inserted a deflated bolus balloon into the esophagus along with our sensor probe and the HRM sensor catheter together. The tips of the two sensor probes were 20–30 cm behind the balloon. We inflated the balloon with 10 mL water and moved it up and down the esophagus. This movement created a swallow reflex, and we recorded the data on both machines before repeating this process twice more with a 5-min break in between. Once we finished with the bolus balloon, we ran tests with a dilation catheter. We inserted the sensor band, HRM sensor, and dilation catheter together roughly 20–30 cm into the esophagus. Using a syringe, we changed the volume of the dilation catheter by increasing it to 10 mL and then decreasing it back to 0 mL. Each of these cycles took 30–60 s. Like the bolus balloon, we conducted three cycles with a 5-min wait between each cycle.

Rectum

We inserted a bolus balloon into the rectum along with the HRM probe and our sensor probe. The two probes were inserted 10 cm into the rectum. We started collecting data and recorded 1 min of a baseline on both devices. At 80s, we inserted the bolus balloon into the rectum with a depth of 5 cm. Then we inflated the balloon with 20 mL of water at 140 s and held it for 2 min. We deflated the balloon and held it for 2 min. We repeated this process two more times.

STATISTICAL ANALYSIS

No data were excluded from the analysis. T tests were performed on MATLAB. A p value <0.05 was considered statistically

significant. The number of replicates used in each study is indicated in the main text. Figure captions define the average value and standard deviation present in the plots.

SUPPLEMENTAL INFORMATION

Supplemental information can be found online at <https://doi.org/10.1016/j.device.2023.100010>.

ACKNOWLEDGMENTS

We thank K. Nan for discussion on electronic designs. We thank J. Hunter, S. Hudson, and M.J. Tarkanian for helping with the bronze casting. We thank S. Srinivasan for help on the *in vivo* testing. We thank D. Mankus from the Koch Institute for Integrative Cancer Research at MIT's Nanotechnology Materials Lab for preparing the SEM images. We thank K. Dobson for review of the manuscript. This work was supported by the Karl van Tassel (1925) Career Development Professorship and the Department of Mechanical Engineering, MIT. N.Z.J. was supported by the Whitaker Health Sciences Fund fellowship and the T. S. Lin fellowship. Q.G., M.Z., J.G.-A., and S.E.W. were supported by the MIT Undergraduate Research Opportunities Program (UROP). V.S. was supported by the University of Wollongong, Australia study leave program.

AUTHOR CONTRIBUTIONS

N.Z.J. and G.T. devised the concept and developed the device. N.Z.J. and Q.G. developed the electronics of the system, computational algorithms, and the printed circuit boards. Q.G. is the co-first author of the paper. N.Z.J., Q.G., V.S., and M.Z. performed sensing material synthesis and characterization. N.Z.J., Q.G., M.Z., J.G.-A., S.E.W., and G.S. fabricated parts for the device. N.Z.J., M.Z., J.L.P.K., J.J., K.I., A.M.H., W.A.M.M., N.F., and K.B.R. designed and performed *in vivo* studies. N.Z.J., Q.G., V.S., M.Z., S.O., and G.T. wrote the paper. All authors discussed the results and commented on the manuscript.

DECLARATION OF INTERESTS

N.Z.J. and G.T. are co-inventors on a patent application related to the work. G.T. has equity and/or stock in Pavoda, Lyndra, Suono Bio, Vivtex, Celero Systems, Bilayer Therapeutics, Inc., Teal Bio, Inc., Syntis Bio, and Vitakey. G.T. is or has served as an advisor for Pavoda, Lyndra, Egalet, Suono Bio, Vivtex, Celero Systems, Bilayer Therapeutics, Inc., Teal Bio, Inc., Syntis Bio, Vitakey, and Kenneth Rainin. G.T. is or has served as a consultant for Pavoda, Entrega, Inc., CBSET, Avaxia, Novo Nordisk, SNS Nano, Egalet, Janssen, Synlogic, Merck, Verily, Eagle Pharmaceuticals, Inc., Wired Consulting, Avadel Pharmaceuticals, Moderna, Syntis Bio, and Vitakey. G.T. receives or has received royalties from Exact Sciences, Horizon, Lyndra, Suono Bio, Vivtex, Celero Systems, Bilayer Therapeutics, Inc., Teal Bio, Inc., Johns Hopkins University, MIT, and Mass General Brigham Innovation. G.T. received gifts from BMS. G.T. received grants and/or scholarships from Novo Nordisk; Hoffman la Roche; Freenome; Oracle; CSL Vifor; the Draper Laboratory; the MIT Lincoln Laboratory; NIH/NIBIB; the Bill and Melinda Gates Foundation; NIH/NCI; the Cambridge Commonwealth and Overseas Trust, University of Cambridge; the Foulkes Foundation; Trinity College, University of Cambridge; the Leona M. and Harry B. Helmsley Charitable Trust; Karl van Tassel (1925) Career Development Professorship, MIT; and the Defense Advanced Research Projects Agency. Complete details of all relationships for profit and not for profit for G.T. can be found at the following link: <https://www.dropbox.com/sh/szi7vnr4a2ajb56/AABs5N5i0q9Aft1IqJAE-T5a?dl=0>.

Received: March 16, 2023

Revised: May 1, 2023

Accepted: June 14, 2023

Published: July 21, 2023

REFERENCES

- Ferrua, M.J., and Singh, R.P. (2011). Understanding the fluid dynamics of gastric digestion using computational modeling. *Procedia Food Sci.* 1, 1465–1472. <https://doi.org/10.1016/j.profoo.2011.09.217>.
- Brandstaeter, S., Fuchs, S.L., Aydin, R.C., and Cyron, C.J. (2019). Mechanics of the stomach: A review of an emerging field of biomechanics. *GAMM Mitt.* 42. <https://doi.org/10.1002/gamm.201900001>.
- Boland, M. (2016). Human digestion – a processing perspective. *J. Sci. Food Agric.* 96, 2275–2283. <https://doi.org/10.1002/jsfa.7601>.
- Tack, J., Demedts, I., Meulemans, A., Schuurkes, J., and Janssens, J. (2002). Role of nitric oxide in the gastric accommodation reflex and in meal induced satiety in humans. *Gut* 51, 219–224. <https://doi.org/10.1136/gut.51.2.219>.
- Banerjee, S., Pal, A., and Fox, M. (2020). Volume and position change of the stomach during gastric accommodation and emptying: A detailed three-dimensional morphological analysis based on MRI. *Neuro Gastroenterol. Motil.* 32, e13865. <https://doi.org/10.1111/nmo.13865>.
- Houghton, L.A., Read, N.W., Heddl, R., Maddern, G.J., Downton, J., Toouli, J., and Dent, J. (1988). Motor activity of the gastric antrum, pylorus, and duodenum under fasted conditions and after a liquid meal. *Gastroenterology* 94, 1276–1284. [https://doi.org/10.1016/0016-5085\(88\)90664-6](https://doi.org/10.1016/0016-5085(88)90664-6).
- Deloose, E., Janssen, P., Depoortere, I., and Tack, J. (2012). The migrating motor complex: control mechanisms and its role in health and disease. *Nat. Rev. Gastroenterol. Hepatol.* 9, 271–285. <https://doi.org/10.1038/nrgastro.2012.57>.
- Marciani, L., Gowland, P.A., Fillery-Travis, A., Manoj, P., Wright, J., Smith, A., Young, P., Moore, R., and Spiller, R.C. (2001). Assessment of antral grinding of a model solid meal with echo-planar imaging. *Am. J. Physiol. Gastrointest. Liver Physiol.* 280, G844–G849. <https://doi.org/10.1152/ajpgi.2001.280.5.G844>.
- Antunes, C., Aleem, A., and Curtis, S.A. (2021). Gastroesophageal reflux disease. In *StatPearls* (StatPearls Publishing).
- Bharucha, A.E., and Lacy, B.E. (2020). Mechanisms, evaluation, and management of chronic constipation. *Gastroenterology* 158, 1232–1249.e3. <https://doi.org/10.1053/j.gastro.2019.12.034>.
- Pandolfino, J.E., and Kahrilas, P.J.; American Gastroenterological Association (2005). American Gastroenterological Association medical position statement: Clinical use of esophageal manometry. *Gastroenterology* 128, 207–208. <https://doi.org/10.1053/j.gastro.2004.11.007>.
- Kim, K.H., Yu, C.S., Yoon, Y.S., Yoon, S.N., Lim, S.-B., and Kim, J.C. (2011). Effectiveness of biofeedback therapy in the treatment of anterior resection syndrome after rectal cancer surgery. *Dis. Colon Rectum* 54, 1107–1113. <https://doi.org/10.1097/DCR.0b013e318221a934>.
- Wiwanitkit, S., and Wiwanitkit, V. (2013). Anorectal manometry and Hirschsprung's disease. *Afr. J. Paediatr. Surg.* 10, 293.
- Lenglinger, J. (2012). Impedance planimetry. In *Dysphagia: Diagnosis and Treatment Medical Radiology*, O. Ekberg, ed. (Springer), pp. 329–337. https://doi.org/10.1007/174_2012_640.
- Maurer, A.H., and Parkman, H.P. (2006). Update on gastrointestinal scintigraphy. *Semin. Nucl. Med.* 36, 110–118. <https://doi.org/10.1053/j.seminuclmed.2005.12.003>.
- Carter, D., and Bardan, E. (2018). The wireless motility capsule. In *Gastrointestinal Motility Disorders: A Point of Care Clinical Guide*, E. Bardan and R. Shaker, eds. (Springer International Publishing), pp. 373–378. https://doi.org/10.1007/978-3-319-59352-4_34.
- Tran, K., Brun, R., and Kuo, B. (2012). Evaluation of regional and whole gut motility using the wireless motility capsule: relevance in clinical practice. *Therap. Adv. Gastroenterol.* 5, 249–260. <https://doi.org/10.1177/1756283X12437874>.
- Enck, P., Azpiroz, F., Boeckxstaens, G., Elsenbruch, S., Feinle-Bisset, C., Holtmann, G., Lackner, J.M., Ronkainen, J., Schemann, M., Stengel, A.,

- et al. (2017). Functional dyspepsia. *Nat. Rev. Dis. Primers* 3, 17081. <https://doi.org/10.1038/nrdp.2017.81>.
19. Du, P., O'Grady, G., Egbuji, J.U., Lammers, W.J., Budgett, D., Nielsen, P., Windsor, J.A., Pullan, A.J., and Cheng, L.K. (2009). High-resolution mapping of in vivo gastrointestinal slow wave activity using flexible printed circuit board electrodes: methodology and validation. *Ann. Biomed. Eng.* 37, 839–846. <https://doi.org/10.1007/s10439-009-9654-9>.
 20. Angeli, T.R., O'Grady, G., Paskaranandavivel, N., Erickson, J.C., Du, P., Pullan, A.J., Bissett, I.P., and Cheng, L.K. (2013). Experimental and automated analysis techniques for high-resolution electrical mapping of small intestine slow wave activity. *J. Neurogastroenterol. Motil.* 19, 179–191. <https://doi.org/10.5056/jnm.2013.19.2.179>.
 21. Cheng, L.K., Du, P., and O'Grady, G. (2013). Mapping and modeling gastrointestinal bioelectricity: from engineering bench to bedside. *Physiology* 28, 310–317. <https://doi.org/10.1152/physiol.00022.2013>.
 22. Lammers, W.J.E.P., Ver Donck, L., Schuurkes, J.A.J., and Stephen, B. (2005). Peripheral pacemakers and patterns of slow wave propagation in the canine small intestine in vivo. *Can. J. Physiol. Pharmacol.* 83, 1031–1043. <https://doi.org/10.1139/y05-084>.
 23. O'Grady, G., Du, P., Paskaranandavivel, N., Angeli, T.R., Lammers, W.J.E.P., Asirvatham, S.J., Windsor, J.A., Farrugia, G., Pullan, A.J., and Cheng, L.K. (2012). Rapid high-amplitude circumferential slow wave propagation during normal gastric pacemaking and dysrhythmias: Circumferential gastric slow wave propagation. *Neuro Gastroenterol. Motil.* 24, e299–e312. <https://doi.org/10.1111/j.1365-2982.2012.01932.x>.
 24. Woodley, F.W., Hayes, D., Kopp, B.T., Moore-Clingenpeel, M., Machado, R.S., Nemastil, C.J., Jadcherla, S., Di Lorenzo, C., Kaul, A., and Mousa, H. (2019). Gastroesophageal reflux in cystic fibrosis across the age spectrum. *Transl. Gastroenterol. Hepatol.* 4, 69. <https://doi.org/10.21037/tgh.2019.08.11>.
 25. Tacheci, I., Květina, J., Kuneš, M., Varayil, J.E., Ali, S.M., Pavlík, M., Kopáčová, M., Rejchrt, S., Bureš, J., and Pleskot, M. (2011). Electrogastrography in experimental pigs: The influence of gastrointestinal injury induced by dextran sodium sulphate on porcine gastric erythromycin-stimulated myoelectric activity. *Neuro Endocrinol. Lett.* 32, 131–136.
 26. Arkwright, J.W., Blenman, N.G., Underhill, I.D., Maunder, S.A., Szczesniak, M.M., Dinning, P.G., and Cook, I.J. (2009). In-vivo demonstration of a high resolution optical fiber manometry catheter for diagnosis of gastrointestinal motility disorders. *Opt. Express* 17, 4500–4508. <https://doi.org/10.1364/OE.17.004500>.
 27. Ruiz-Vargas, A., Costa, M., Wiklendt, L., Dinning, P.G., and Arkwright, J.W. (2015). The use of fibre optic sensing technology with intraluminal impedance catheter for functional gastrointestinal motility disorders. <https://doi.org/10.13140/RG.2.1.3125.9124>.
 28. Arkwright, J.W., Blenman, N.G., Underhill, I.D., Maunder, S.A., Lim, B., Szczesniak, M.M., Dinning, P.G., Cook, I.J., and Doe, S.N. (2008). The use of wavelength division multiplexed fiber Bragg grating sensors for distributed sensing of pressure in the gastrointestinal tract. In 2008 IEEE PhotonicsGlobal@Singapore, pp. 1–4. <https://doi.org/10.1109/IPGC.2008.4781397>.
 29. Tomek, J., Mlejnek, P., Janásek, V., Ripka, P., Kašpar, P., and Chen, J. (2007). Gastric motility and volume sensing by implanted magnetic sensors. *Sens. Lett.* 5, 276–278. <https://doi.org/10.1166/sl.2007.002>.
 30. Dimoulas, C., Kalliris, G., Papanikolaou, G., Petridis, V., and Kalampakas, A. (2008). Bowel-sound pattern analysis using wavelets and neural networks with application to long-term, unsupervised, gastrointestinal motility monitoring. *Expert Syst. Appl.* 34, 26–41. <https://doi.org/10.1016/j.eswa.2006.08.014>.
 31. Silva, L.R., Sousa, P.J., Goncalves, L.M., and Minas, G. (2015). Flexible gastrointestinal motility pressure sensors based on aluminum thin-film strain-gauge arrays. *J. Microeng. Microtech.* 25, 074007. <https://doi.org/10.1088/0960-1317/25/7/074007>.
 32. Paixão, F.C., Corá, L.A., Américo, M.F., de Oliveira, R.B., Baffa, O., and Miranda, J.R.A. (2012). Development of an AMR-ACB array for gastrointestinal motility studies. *IEEE Trans. Biomed. Eng.* 59, 2737–2743. <https://doi.org/10.1109/TBME.2012.2208748>.
 33. Dagdeviren, C., Javid, F., Joe, P., von Erlach, T., Bense, T., Wei, Z., Saxton, S., Cleveland, C., Booth, L., McDonnell, S., et al. (2017). Flexible piezoelectric devices for gastrointestinal motility sensing. *Nat. Biomed. Eng.* 1, 807–817. <https://doi.org/10.1038/s41551-017-0140-7>.
 34. A gastric resident drug delivery system for prolonged gram-level dosing of tuberculosis treatment | *Sci. Transl. Med.* <https://www.science.org/doi/full/10.1126/scitranslmed.aau6267>.
 35. Stoeckel, D., Pelton, A., and Duerig, T. (2004). Self-expanding nitinol stents: material and design considerations. *Eur. Radiol.* 14, 292–301. <https://doi.org/10.1007/s00330-003-2022-5>.
 36. Bose, A., Hartmann, M., Henkes, H., Liu, H.M., Teng, M.M.H., Szikora, I., Berlis, A., Reul, J., Yu, S.C.H., Forsting, M., et al. (2007). A novel, self-expanding, nitinol stent in medically refractory intracranial atherosclerotic stenoses: the Wingspan study. *Stroke* 38, 1531–1537. <https://doi.org/10.1161/STROKEAHA.106.477711>.
 37. Maleckis, K., Anttila, E., Aylward, P., Poulson, W., Desyatova, A., MacTaggart, J., and Kamenskiy, A. (2018). Nitinol stents in the femoropopliteal artery: a mechanical perspective on material, design, and performance. *Ann. Biomed. Eng.* 46, 684–704. <https://doi.org/10.1007/s10439-018-1990-1>.
 38. Liatsikos, E.N., Karnabatidis, D., Kagadis, G.C., Katsakioti, P.F., Stolzenburg, J.-U., Nikiforidis, G.C., Perimenis, P., and Siablis, D. (2007). Metal stents in the urinary tract. *EAU-EBU Update Ser.* 5, 77–88. <https://doi.org/10.1016/j.eeus.2006.11.003>.
 39. van Dijk, M.M., Mochtar, C.A., Wijkstra, H., Laguna, M.P., and de la Rosette, J.J.M.C.H. (2006). The bell-shaped nitinol prostatic stent in the treatment of lower urinary tract symptoms: Experience in 108 patients. *Eur. Urol.* 49, 353–359. <https://doi.org/10.1016/j.eururo.2005.12.008>.
 40. Mau, M.M., Sarker, S., Harris, S., and Terry, B.S. (2023). Design and testing of a superelastic nitinol tissue attachment mechanism for long-term gastrointestinal device retention. *J. Med. Device.* 17. <https://doi.org/10.1115/1.4057058>.
 41. Iowa State University Digital Press. Swine Health Recommendations: Exhibitors of all pigs going to exhibits or sales MSU extension. https://www.canr.msu.edu/resources/swine_health_recommendations_exhibitors_of_all_pigs_going_to_exhibits_or_sa.
 42. Kuphaldt, T.R., and Haughey, J. (2020). *Electrical Safety*.
 43. Handel, N., and Gutierrez, J. (2006). Long-term safety and efficacy of polyurethane foam-covered breast implants. *Aesthet. Surg. J.* 26, 265–274. <https://doi.org/10.1016/j.asj.2006.04.001>.
 44. Dinu, S., Craciunescu, E.L., Macasoi, I., Chioran, D., Rivis, M., Vlad, D., Milutinovici, R.A., Marcovici, I., Dolghi, A., Moaca, A., et al. (2022). Toxicological assessment of an acrylic removable orthodontic appliance using 2D and 3D in vitro methods. *Materials* 15, 1193. <https://doi.org/10.3390/ma15031193>.
 45. Material Safety Data Sheet (Activated Carbon) Parchem 2009. <https://www.parchem.com/siteimages/Attachment/Activated%20Carbon%20MSDS.pdf>.
 46. Cheeney, G., Nguyen, M., Valestin, J., and Rao, S.S.C. (2012). Topographic and manometric characterization of the recto-anal inhibitory reflex. *Neuro Gastroenterol. Motil.* 24, e147–e154. <https://doi.org/10.1111/j.1365-2982.2011.01857.x>.
 47. Chang, H., Li, S., Li, Y., Hu, H., Cheng, B., Miao, J., Gao, H., Ma, H., Gao, Y., and Wang, Q. (2020). Effect of sedation with dexmedetomidine or propofol on gastrointestinal motility in lipopolysaccharide-induced endotoxemic mice. *BMC Anesthesiol.* 20, 227. <https://doi.org/10.1186/s12871-020-01146-z>.